2016

Real-time Profiling of Solid-State Nanopores During Solution-Phase Nanofabrication

Y. M. N. D. Y. Bandara
University of Rhode Island

Buddini Iroshika Karawdeniya
University of Rhode Island

Jason R. Dwyer
University of Rhode Island, jason_dwyer@uri.edu

Real-time Profiling of Solid-State Nanopores During Solution-Phase Nanofabrication

Real-time Profiling of Solid-State Nanopores During Solution-Phase Nanofabrication.

Y.M. Nuwan D.Y. Bandara, Buddini Iroshika Karawdeniya, and Jason R. Dwyer*.

Real-time Profiling of Solid-State Nanopores During Solution-Phase Nanofabrication.

Y.M. Nuwan D.Y. Bandara, Buddini Iroshika Karawdeniya, and Jason R. Dwyer*.

Department of Chemistry, University of Rhode Island, 140 Flagg Road, Kingston, RI, 02881, United States.

ABSTRACT. We describe a method for simply characterizing the size and shape of a nanopore during solution-based fabrication and surface modification, using only low-overhead approaches native to conventional nanopore measurements. Solution-based nanopore fabrication methods are democratizing nanopore science by supplanting the traditional use of charged-particle microscopes for fabrication, but nanopore profiling has customarily depended on microscopic examination. Our approach exploits the dependence of nanopore conductance in solution on nanopore size, shape, and surface chemistry in order to characterize nanopores. Measurements of the changing nanopore conductance during formation by etching or deposition can be analyzed using our method to characterize the nascent nanopore size and shape—beyond the typical cylindrical approximation—in real-time. Our approach thus accords with ongoing efforts to broaden the accessibility of

nanopore science from fabrication through use: it is compatible with conventional instrumentation and offers straightforward nanoscale characterization of the core tool of the field.

Introduction

A nanopore is a nanofluidic channel, with dimensions in all directions generally less than 100 nm, that can be used to deliver a host of capabilities for single-molecule sensing.[1-10] High-profile nanopore sensing efforts have targeted sequencing single strands of DNA and RNA; protein conformational analysis; and characterization of other biomolecules, molecular complexes, and nanoparticles. In the most straightforward implementation of nanopore sensing, the nanopore is the sole path connecting two reservoirs containing electrolyte solutions. Electrodes in each reservoir establish a potential difference across the nanopore that drives ions through the nanopore: passage of a target molecule, nanoparticle, or complex through the nanopore perturbs that ionic current and provides molecular-level information. That information naturally depends on the target's dimensions and physicochemical properties and the ionic solution composition, but it is also profoundly affected by the size, shape, and surface chemistry of the nanopore. In the case of a (cylinder-like) double-stranded DNA polymer that fills the entire length of a cylindrical nanopore as it transits through, a simple geometric treatment considering only the displacement of bulk ions by the polymer gives a straightforward expression for the macromolecule-induced conductance change[11]

$$\chi_{\mathrm{B}} \equiv \frac{(\langle G \rangle - \langle G_b \rangle)}{\langle G \rangle} \cong \left(\frac{r_{\mathrm{DNA}}}{r_0} \right)^2 \tag{1}$$

with $\langle G \rangle$ and $\langle G_b \rangle$ the time-averaged conductance through an unobstructed and DNA-containing nanopore, respectively, and r_{DNA} and r_0 the cross-sectional radii of the molecule and nanopore. The expression does not capture the panoply of complex phenomena giving rise to conductance

perturbations in nanopore sensing,[12-13] but does, in convenient closed form, appropriately underscore the importance of nanopore dimension. This geometric basis of the conductance change has been used to infer biopolymer conformation, for example: a folded-over polymer presents a larger effective cross-section than a linear one.[14] The more elusive dependence of current change on single-stranded DNA base sequence, for example, underpins efforts to sequence single strands of DNA using nanopores.[2, 8] In a powerful implementation of nanopore force spectroscopy, details of interaction energetics can be revealed if, and only if, a nanopore size is properly engineered to sterically force the linearization of a folded moiety during passage, or rupture of an intermolecular complex by barring passage of one of the partners.[15-17]

The ionic conductance (G), alone, of a nanopore with a charged surface can be expressed as the sum of a bulk and surface conductance term[18-21]

$$G = G_{\text{bulk}} + G_{\text{surface}} = K \cdot A + \mu |\sigma| \cdot B \tag{2}$$

when access resistance is negligible.[22] Overlapping Debye layers require a more sophisticated treatment, but need not be considered over a broad useful range of nanopore sizes and solution ionic strengths.[23-24] This simple formulation for G has been supported by experimental measurements in which nanopore conductance was measured for nanopores that had size and shape interrogated by combinations of transmission electron microscopy and electron energy loss spectroscopy.[13, 18] The bulk conductance is determined by the solution conductivity, K, and a volume integral, A, over the unique nanopore shape: $G_{\text{bulk}} = K \left(\int \frac{dz}{\pi (r(z))^2} \right)^{-1} = K \cdot A$ (with z-axis along the length of the pore). The surface conductance is determined by the mobility of counterions proximal to the pore surface, μ, the density of surface chargeable groups, σ, and an integral, B, over the surface of the nanopore: $G_{\text{surface}} = \mu |\sigma| \left(\int \frac{dz}{2\pi r(z)} \right)^{-1} = \mu |\sigma| \cdot B$. The two defined quantities A and B therefore contain information about the size and shape of the nanopore,

4

determined by the collection of geometric parameters, q_j, relevant for a particular shape: $A = A(\{q_j(t)\})$ and $B = B(\{q_j(t)\})$. Nanopore materials are usually chosen with mechanical and physicochemical properties to minimize the change in size and shape in time, t, absent deliberate action. Commonly reported parameter values, which may be only a subset of those needed to fully characterize a given nanopore profile, include the limiting radius (the minimum radius along the profile), r_0, and total nanopore length, L, that can in some cases be equated with the supporting membrane thickness. The experimentally-supported[13, 18] treatment of the nanopore conductance here assumes axially and cylindrically symmetric nanopores in a size regime where access resistance is negligible,[22] and that any surface charge emerges from a singly ionizable surface species described by a characteristic pK_a

$$-A - H \rightleftharpoons -A^- + H^+ \tag{3}$$

Native or engineered nanopore surface chemistry is an important element in nanopore performance, and contributor to nanopore conductance. The conductance can be naturally exploited for nanopore characterizations in conjunction with solution-based nanopore fabrication methods, and is especially useful when more complex methods present barriers to use. Charged-particle milling is an established, but challenging and burdensome, approach for formation of the smallest, <10 nm nanopores in thin membranes.[25-28] The use of (scanning) transmission electron microscopes ((S)TEM), helium ion microscopes, and scanning electron microscopes (SEM) for fabrication imposes time and instrumentation costs; can expose the nanopore to possible surface contamination within the instrument and to risk of damage during handling, transfer, and charged particle beam exposure; and reveals little of the nanopore surface chemistry. In a purely imaging capacity, these microscopes are limited in their ability to characterize organic surface coatings, and without more involved measurements or image analysis,[18, 29-34] yield only a nanopore limiting

radius—not a fully characterized size and shape. Beyond the greater ease and technical benefits of a low-overhead, solution-based nanopore characterization, such an approach can more directly probe nanopore surface chemistry. The capabilities of solution-based nanopore fabrication make a strong case alone, however, for complementary solution-based characterization methods. The benefits and prospects of solution-based nanopore fabrication were demonstrated early-on in the field through the development and use of track-etched polymer nanopores.[9] Formation of the etchant-susceptible ion-track requires a large-scale heavy ion accelerator facility which naturally imposes a barrier to widespread use of the fabrication method, although accessibility is improved by the ability to perform the solution-based chemical etching step in a standard chemistry lab well after the ion-track formation. Conformal metal coating of these often tortuous polymer nanopores by (solution-based) electroless plating was a vital development in the use of these polymer nanopores: the material deposition allows the nanopore dimensions to be fine-tuned after chemical etching, and the metal film provides a platform for subsequent chemical modification of the nanopore interior surface. Both etching and deposition steps developed for polymer membrane nanopores have been extended to silicon nitride membranes which offer benefits such as the fabrication of smooth nanopores with lengths <100 nm.[32, 35] More recently, dielectric breakdown (followed by voltage-assisted etching) of an impervious, insulating membrane, has emerged as a powerful new technique for nanopore fabrication.[36] It is an entirely solution-based approach, using essentially the same equipment required for conductance-based nanopore measurements, and quite readily produces nanopores in a wide range of sizes, including in the coveted <5 nm diameter range. The nanopore conductance can be measured during fabrication, providing an indication of the nanopore size at a given point in time. The dielectric breakdown approach allows nanopores to be fabricated in their native environment, in the same holder where they will be used for

experiments, and without the contamination and damage risks associated with charged particle techniques. A conductance-based characterization will not damage a molecular surface coating suitable for conductance-based sensing, and can harness the natural and direct connection to the nanopore surface chemistry that makes it a valuable method for characterizing chemically-tailored nanopores.[9, 23, 34, 37] The conductance model is equally useful when a pore is formed and enlarged, and when an initially large pore is resized by solution-based deposition, including film growth.[9, 19, 35, 38] Etching and deposition may be used in concert, with a pore being initially etched larger than desired to accommodate an electroless gold film, for example, that may ease nanopore surface chemical modification. In this work we wanted to understand how the measured conductance during nanopore fabrication—by deliberate expansion, closure, or both in consort—could be used to profile the nascent nanochannel. Simulations will focus, for expediency, on nanopores fabricated via deposition of surface coatings: the principles, however, are general.

Theory

The algebraic structure of $G = K \cdot A + \mu |\sigma| \cdot B$, and its underlying dependencies, means that a single-point conductance measurement can provide enough information to size a nanopore only when the shape is known and the fitting involves only a single geometric degree of freedom. Measurement of G versus K—by changing the electrolyte solution conductivity—for a given nanopore can provide greater insight into the nanopore size, shape, and surface chemistry.[18, 21-23] The conductance change after adding a monolayer of known thickness, for example, can provide similar information to what is provided after a solution conductivity change, and measuring G versus K for the nanopore before and after monolayer formation provides the richest description of the nanopore within this framework.[23] Changes of electrolyte solution are tedious, however, and disruptive to a solution-based nanopore fabrication approach. A simple ongoing measurement of

the nanopore conductance during nanopore formation, however, can be done as part of the fabrication process, and is in fact performed routinely on a single-point measurement basis. Each fixed-time conductance is of course connected through Equation (2) to the instantaneous nanopore size and shape, where the applicability of the conductance model has been independently verified by electron-based imaging and spectroscopy.[13, 18] A single conductance value, however, offers a limited ability to characterize a nanopore described by more than one free geometric parameter. Measurement and use of a series of conductance values at times t_i: $G(t_0, \{q_j(t_0)\})$, $G(t_1, \{q_j(t_1)\}), \ldots G(t_n, \{q_j(t_n)\})$, can provide more information than the conductance at a single time-point since the changes in conductance are caused by underlying changes in the initial nanopore dimensions, $\{q_j(t_0)\}$, in time. We perform simulations consistent with the following conditions to demonstrate how to extract this information content. Nanometer-scale deposition or etching should not appreciably change the electrolyte solution conductivity, nor should the nanopore surface chemistry change (except through deliberate action) throughout either type of fabrication process. We make the reasonable assumption that material transfer will be uniform across the surface, so that the nanopore shape will remain unchanged. Silicon nitride, the most common membrane material in which to form nanopores, is amorphous, and so will not inherently be prone to anisotropic etching.[39] Electroless plating, a surface deposition method that has been used with great success in resizing nanopores,[9] conformally coats even rough surfaces,[40] and film growth by polymer chain extension, for example, should be another effective route to reliably tune nanopore size.[41] We can then write

$$\frac{dG}{dt} = K \frac{dA(\{q_j(t)\})}{dt} + \mu |\sigma| \frac{dB(\{q_j(t)\})}{dt} = K \sum_j \left(\frac{\partial A}{\partial q_j}\right) \frac{dq_j}{dt} + \mu |\sigma| \sum_j \left(\frac{\partial B}{\partial q_j}\right) \frac{dq_j}{dt} =$$
$$K \sum_j f(\{q_j\}, v_{mt}, t) + \mu |\sigma| \sum_j g(\{q_j\}, v_{mt}, t) \qquad (4)$$

where the $\left(\frac{\partial A}{\partial q_j}\right)$ and $\left(\frac{\partial B}{\partial q_j}\right)$ depend on the nanopore profile, and the $\frac{dq_j}{dt}$ depend on the profile and the material transfer rate, v_{mt}, whether by nanopore etching or coating by deposition. The material transfer rate is conveniently measured as the change in nanopore radius over time. While two nanopores with different shapes and sizes may have the same initial conductance, $G(t_0, \{q_j(t_0)\}) = G(t_0, \{q'_j(t_0)\})$, the rates of change of the conductances will be different, and determined by the individual nanopore sizes and shapes (and identical material transfer rates). Measurement of several values of the experimental $G(t_i, \{q_j(t_i)\})$ can use this dependence to enhance real-time conductance-based nanopore characterization during fabrication. To present concrete examples of the general framework, we selected four representative nanopore profiles: cylindrical, double-conical, conical-cylindrical, and hyperbolic (Figure 1).[18, 21-22, 29, 32] For all profiles, we limited the $\{q_j\}$ to two free parameters per shape: (r_0, L)—the limiting (minimum) radius and total nanopore length (see Tables S-1 and S-2 for notation and equations). Independent experimental studies of nanopore profiles[18, 22] were used to guide the constraints and to make reasonable parameter value assignments to allow for numerical examples; the nanopore characterization method is general, however, and does not depend upon these particular numerical values.[21, 23] We restricted the initial outer radius to be 10 nm greater than the initial limiting radius (not applicable to the cylindrical profile),[21-22] and fixed the initial cylinder length of the conical-cylindrical pore to be 0.6 times its initial total length. The deposited coating was piecewise curved to maintain a uniform coating thickness across the entire nanopore surface (Figure 1 and Table S-2). Equation (4) then becomes

$$\frac{dG}{dt} = K\left(\left(\frac{\partial A}{\partial r_0}\right)\frac{dr_0}{dt} + \left(\frac{\partial A}{\partial L}\right)\frac{dL}{dt}\right) + \mu|\sigma|\left(\left(\frac{\partial B}{\partial r_0}\right)\frac{dr_0}{dt} + \left(\frac{\partial B}{\partial L}\right)\frac{dL}{dt}\right) = v_{mt}\left[K\left(\left(\frac{\partial A}{\partial r_0}\right) + 2\left(\frac{\partial A}{\partial L}\right)\right) + \mu|\sigma|\left(\left(\frac{\partial B}{\partial r_0}\right) + 2\left(\frac{\partial B}{\partial L}\right)\right)\right] \quad (5)$$

Parameter values used in calculations were typical of experiments and consistent with those in prior work with silicon nitride nanopores:[21] for example, 1 M potassium chloride electrolyte solution in water, K=14.95 S·m^{-1} (calculated using ion mobilities), pH=7.0, and surface pK$_a$=7.9. The material transfer rate was kept constant, $v_{mt} = dr_0/dt = 0.6$ nm/h. More important than the particular parameter values, though, it is the form of equation (2) and its functional dependencies that are significant in this work.
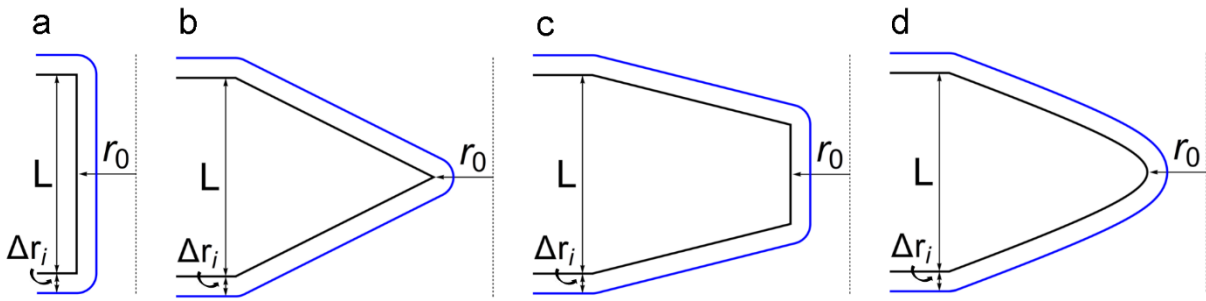

Figure 1. (a) Cylindrical, (b) double-conical, (c) conical-cylindrical, and (d) hyperbolic nanopore half-profile cross-sections cylindrically symmetric about the vertical z-axis (dotted line) of the pore. Profiles are shown before (black line) and after (blue line) material deposition to decrease the limiting nanopore radius, r_0, by an amount Δr_i determined by the deposition time and material transfer rate.

Results and Discussion

The ability to characterize a nanopore in real-time, during its formation, using only its conductance, is an incredibly compelling goal. Its pursuit relies on the connection between the conductance of a nanopore and its size, shape, and surface chemistry, and its attainment hinges on properly exploiting the functional form of that connection. We will focus on nanopores fabricated by deposition of a coating onto the outer membrane surface and inner surface of an existing, larger

pore, but similar arguments hold for a nanopore formed by etching of a smaller pore to create a larger pore. Figure 2 highlights a primary challenge of nanopore conductance-based characterizations. The curves show the set of nanopore limiting radii and length, for each chosen nanopore shape, $\{r_{0,\text{shape}}, L_{\text{shape}}\}$, that generate a 200 nS conductance: there is not a unique solution. To use a single-point conductance value to characterize a nanopore by more than a broad range of possible shapes and sizes, or to provide better than an approximate size given an assumed profile, additional information is required.[21, 23] Most commonly, knowledge of the particular fabrication method and conditions is used to choose an expected nanopore profile, and can often be used to constrain the nanopore length to an experimental parameter such as the thickness of the membrane in which it is formed. Measurement of the conductance of a nanopore in time, in an essentially single-point sense, has demonstrated utility as a monitor of nanopore evolution even if it cannot provide an unambiguous characterization. Yet the time-dependence provides a set of experimental data points that we seek to mine to more fully characterize the nanopore than is possible using a single-point measurement of the conductance.
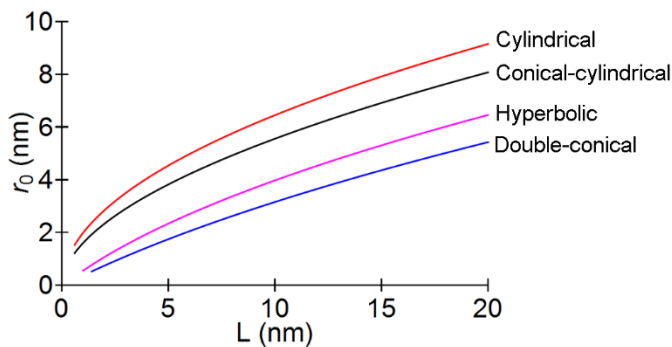

Figure 2. The plotted lines denote the pairings of limiting nanopore radius, r_0, and nanopore length, L, for each nanopore profile, that will produce a 200 nS conductance.

The most immediately striking consequence of a real-time measurement of the conductance is that, as shown in Figure 3, it reveals a clear distinction between different nanopore profiles. When different candidate profiles are used to fit experimental nanopore conductance data, the conductance versus time provides a means to determine nanopore shape and size. To produce the data plotted in Figure 3, we used the four representative nanopore profiles all with an initial 200 nS conductance and 10 nm total nanopore length. The initial nanopore limiting radii were ~6.4, 3.1, 5.5, and 4.0 nm, respectively, for the cylindrical, double-conical, conical-cylindrical, and hyperbolic nanopore profiles. We calculated the conductance for each profile as the radii were reduced at the same rate, $v_{mt} = 0.6$ nm/h, during a simulated, deposition-based fabrication process. As shown below, the radius change after a given time must be known, but the method does not require a constant material transfer rate. We chose a constant rate, commonly observed in micromachining processing,[39] however, because it affords straightforward insights into the functional dependencies beyond what is revealed by the numerical results. Given the form of equation (5), it is perhaps unsurprising that even with constant v_{mt} (and therefore identical absolute rates of change of the radii across profile type), $\frac{dG}{dt}$ is not linear and depends on profile type (inset of Figure 3). The quantitative details of this behavior provide a means of extracting nanopore size and shape information from the measured conductance changes. Figure S-2 reinforces the geometrical underpinnings of this profiling method, in plots of the geometry integrals, *A* and *B*, versus time.
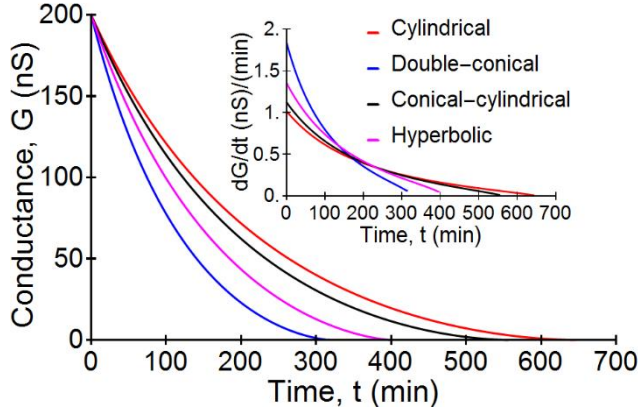
Figure 3. Nanopores with an initial 200 nS conductance ($L(t_0) = 10$ nm, $r_0(t_0)$ from Figure 2) show a shape-dependent decrease in conductance due to material deposition at a constant rate, v_{mt}. The inset plots the rate of conductance change, calculated using nearest-neighbor differences, $\frac{dG}{dt} \cong \frac{G(t_{i+1}) - G(t_i)}{t_{i+1} - t_i}$.

Figure 4 illustrates the general approach we have adopted for extracting quantitative nanopore geometric parameters from $G(t)$—an approach allowing for a nanopore characterization with the full geometric parameter flexibility outlined in Figure 2, and that emphasizes the minimal number of conductance values required. We chose to simulate the deposition-based fabrication of nanopores with an initial conductance, $G_{\text{shape}}^{\text{expt}}(t_0) = 200 \ nS$, and initial radius, $r_{0,\text{shape}}^{\text{expt}}(t_0) = 3.5$ nm (both values the same for all simulated experimental shapes); Figure 2 gives the corresponding initial nanopore lengths, $L_{\text{shape}}^{\text{expt}}(t_0)$, for each nanopore profile. For each nanopore profile, we set the initial nanopore size, $\left(r_{0,\text{shape}}^{\text{expt}}(t_0), L_{\text{shape}}^{\text{expt}}(t_0)\right)$, and used the progression of dimensions, $\left(r_{0,\text{shape}}^{\text{expt}}(t_0) - \Delta r_i(t_0, t_i), L_{\text{shape}}^{\text{expt}}(t_0) + 2\Delta r_i(t_0, t_i)\right)$, to simulate the post-deposition

13

conductances $G_{\text{shape}}^{\text{expt}}(t_1)$ and $G_{\text{shape}}^{\text{expt}}(t_2)$. For a constant material transfer rate, v_{mt}, $\Delta r_i = (t_i - t_0)v_{mt}$. While more generally $\Delta r_i = \Delta r_i(t_i, t_0, v_{mt}(t))$, the procedure implemented here relies on knowledge of this radius change only, not whether the material transfer rate is constant in time or not. We outline the conceptual framework for the characterization and provide a detailed step-by-step tutorial in the SI. The initial conductance, $G_{\text{shape}}^{\text{expt}}(t_0)$, was used in conjunction with Figure 2 to establish the set of candidate $\left\{\left(r_{0,\text{shape}}(t_0), L_{\text{shape}}(t_0)\right)\right\}$, for each nanopore profile, whose members all have the initial conductance $G_{shape}(t_0) = G_{\text{shape}}^{\text{expt}}(t_0)$. The range of candidate sizes, for each candidate shape, is represented by the dotted lines in Figure 4a-d. Given $G_{\text{shape}}^{\text{expt}}(t_0)$, alone, neither size nor shape can yet be determined. Each of these possible candidate geometries (size and shape) was then modified by the deposition of material to provide sets of nanopore dimensions given by $\left\{\left(r_{0,\text{shape}}(t_0) - \Delta r_i, L_{\text{shape}}(t_0) + 2\Delta r_i\right)\right\}$ for times t_1, t_2, and t_3, with corresponding sets of conductances $\left\{G_{\text{shape}}(t_1)\right\}$, $\left\{G_{\text{shape}}(t_2)\right\}$, and $\left\{G_{\text{shape}}(t_1)\right\}$ (solid curves in Figure 4a-d). We then used the post-deposition $G_{\text{shape}}^{\text{expt}}(t_i)$ to determine the nanopore size and shape. We found the initial limiting radius, $r_{0,\text{shape}}(t_0)$, for each nanopore shape, that gave a conductance $G_{shape}(t_1) = G_{\text{shape}}^{\text{expt}}(t_1)$. That is, when the experimental nanopore was cylindrical, we found the $r_{0,\text{shape}}(t_0)$ for cylindrical, double-conical, conical-cylindrical, and hyperbolic profiles that allowed the candidate pore conductance to match the experimental value, and plotted the radii in Figure 4e. Figure 4f-h are plots of the $r_{0,\text{shape}}(t_0)$ when the conductances of double-conical, conical-cylindrical, and hyperbolic experimental nanopores were equated to the conductances of the same four candidate shapes. No matter the experimental profile, after two conductance values, all four candidate shapes—with different sizes—were equally viable

conductance-based matches. By repeating this process by finding $r_{0,\text{shape}}(t_0)$ to satisfy $G_{\text{shape}}(t_2) = G_{\text{shape}}^{\text{expt}}(t_2)$, the experimental nanopore size and shape both emerge. When the candidate nanopore profile matches the simulated experimental profile, all extracted $r_{0,\text{shape}}(t_0)$ have the same value for all t_i, which essentially delivers a simultaneous solution of $G_{\text{shape}}\big(t_i, \{q_j(t_i)\}\big) = G_{\text{shape}}^{\text{expt}}\big(t_i, \{q_j(t_i)\}\big)$ for all time-points. The curves in Figure 4e-h illustrate this successful characterization; the agreement is shown in terms of $r_{0,\text{shape}}(t_0)$, but $L_{\text{shape}}(t_0)$ has the same behavior. Figure 4e plots the $r_{0,\text{shape}}(t_0)$ when the simulated $G_{\text{cylindrical}}^{\text{expt}}(t_i)$ values were fit using cylindrical, double-conical, conical-cylindrical, and hyperbolic profiles: only the cylindrical candidate nanopore returns the same $r_{0,\text{shape}}(t_0)$ for different t_i. Figures 4f-h show, by the constancy of the correct $r_{0,\text{shape}}(t_0)$, the same successful capture of size and shape of double-conical, conical-cylindrical, and hyperbolic simulated experimental nanopores, respectively. Measurement of more conductance points does not provide more information, given the framework presented here, but can add numerical robustness to this approach. Alternatively, the formal need for only three conductance values allows one to piecewise repeat the shape-and size-profiling on independent sets of three conductance values throughout the duration of the fabrication, allowing for the possibility to extend this method to anisotropically-etching or -depositing materials. An extreme departure from the usual progression of conductance in time may signal the need for a more involved steady-state solution-based characterization of a pore after fabrication,[21] although even in this case the present time-dependent method should provide bounds on the evolving nanopore size. We note again, for generality, that while we used a constant v_{mt}, the plating rate must be known, but need not be constant. Fitting conductance values in time leverages the form of equation (2) to reveal the nanopore shape and extract dimensions from a solution-based nanopore fabrication method.
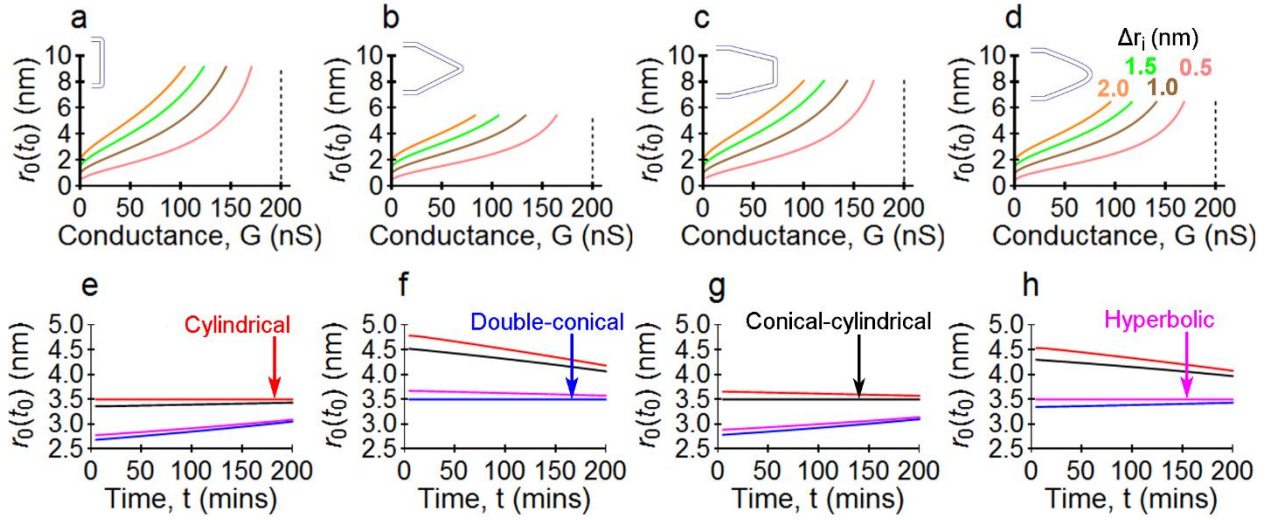
Figure 4. The conductance of initially 200 nS (a) cylindrical, (b) double-conical, (c) conical-cylindrical, and (d) hyperbolic nanopores can be satisfied by a range of radii (dotted vertical lines). Fixed decreases of each possible radius (in time) generate characteristic conductance progressions that depend on the nanopore shape and initial size (conductance curves labelled with their particular Δr_i). Simulated experimental conductance data versus time for $G_{\text{shape}}^{\text{expt}}(t_0) = 200$ nS, $r_{0,\text{shape}}(t_0) = 3.5$ nm pores of each shape were compared to the plots in (a-d) to reveal the (e) cylindrical (red), (f) double-conical (blue), (g) conical-cylindrical (black), and (h) hyperbolic (magenta) experimental nanopore size and shapes by the constancy of the fitting $r_{0,\text{shape}}(t_0)$. The relevant experimental profiles for each column are inset in the top row.

Conclusions

The charged-particle, complex instrumentation approaches that dominated early nanopore fabrication methods allowed, in principle, for high-resolution nanopore characterizations, although such capability was rarely employed beyond determining a limiting radius. These instrumental approaches face limitations such as high likelihood of surface contamination and inability to probe

soft (e.g. organic) nanopore coatings, and they add workflow steps that could be costly in time and instrumentation. Even so, since the nanopores were formed in these instruments, it was expedient to follow fabrication with the chosen degree of characterization in the same instrument. The ongoing development of completely solution-based methods—including the advent of new techniques—to fabricate nanopores has ushered in an exciting new area for nanofluidics, generally, and nanopore science in particular. Nanopores can now be formed in their native liquid environment, and without the instrument and workflow cost of charged-particle methods. We have modelled the nanopore conductance with a simple framework that nevertheless includes an explicit surface chemistry term and has demonstrated concordance with independent experimental characterizations of nanopore sizes and shapes of most importance for routine use in single molecule science.[13, 18] We have presented theoretical examples that describe the creation of small nanopores by coating larger nanopores, so that fabrication involves a decrease in the nanopore radius and conductance. The results, however, are equally applicable to nanopore fabrication methods such as dielectric breakdown followed by voltage-assisted etching, or the chemical etching of ion-tracked membranes. The nanopore conductance is routinely measured during dielectric breakdown as a diagnostic, and such a measurement can be readily implemented during nanopore fabrication by material deposition. We have shown here that by analyzing a series of conductance measurements in time, rather than only an instantaneous measurement, we are able to extract information on nanopore size and shape, and thereby enrich the execution and interpretation of nanopore experiments without increasing the experimental burden.

ASSOCIATED CONTENT

Supporting Information. Detailed descriptions of nanopore profiles and a step-by-step tutorial detailing the numerical nanopore characterization. This material is available free of charge via the Internet at http://pubs.acs.org.

AUTHOR INFORMATION

Corresponding Author

*E-mail: jdwyer@chm.uri.edu

Author Contributions

The manuscript was written through contributions of all authors. All authors have given approval to the final version of the manuscript.
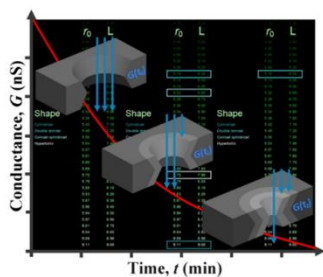
ABBREVIATIONS

min., minutes; h, hours.

REFERENCES

1.   Haywood, D. G.; Saha-Shah, A.; Baker, L. A.; Jacobson, S. C., Fundamental Studies of Nanofluidics: Nanopores, Nanochannels, and Nanopipets. *Anal. Chem.* **2015,** *87*, 172-187.

2.   Taniguchi, M., Selective Multidetection Using Nanopores. *Anal. Chem.* **2015,** *87*, 188-199.

3.   Reiner, J. E.; Balijepalli, A.; Robertson, J. W. F.; Campbell, J.; Suehle, J.; Kasianowicz, J. J., Disease Detection and Management Via Single Nanopore-Based Sensors. *Chem. Rev.* **2012,** *112*, 6431-6451.

4.   Howorka, S.; Siwy, Z., Nanopore Analytics: Sensing of Single Molecules. *Chem. Soc. Rev.* **2009,** *38*, 2360-2384.

5.   Miles, B. N.; Ivanov, A. P.; Wilson, K. A.; Dogan, F.; Japrung, D.; Edel, J. B., Single Molecule Sensing with Solid-State Nanopores: Novel Materials, Methods, and Applications. *Chem. Soc. Rev.* **2013,** *42*, 15-28.

6.   Kudr, J.; Skalickova, S.; Nejdl, L.; Moulick, A.; Ruttkay–Nedecky, B.; Adam, V.; Kizek, R., Fabrication of Solid-State Nanopores and Its Perspectives. *ELECTROPHORESIS* **2015,** *36*, 2367-2379.

7.   Oukhaled, A.; Bacri, L.; Pastoriza-Gallego, M.; Betton, J.-M.; Pelta, J., Sensing Proteins through Nanopores: Fundamental to Applications. *ACS Chemical Biology* **2012,** *7*, 1935-1949.

8.   Branton, D.; Deamer, D. W.; Marziali, A.; Bayley, H.; Benner, S. A.; Butler, T.; Di Ventra, M.; Garaj, S.; Hibbs, A.; Huang, X. H.; Jovanovich, S. B.; Krstic, P. S.; Lindsay, S.; Ling, X. S. S.; Mastrangelo, C. H.; Meller, A.; Oliver, J. S.; Pershin, Y. V.; Ramsey, J. M.; Riehn, R.; Soni, G. V.; Tabard-Cossa, V.; Wanunu, M.; Wiggin, M.; Schloss, J. A., The Potential and Challenges of Nanopore Sequencing. *Nat. Biotechnol.* **2008,** *26*, 1146-1153.

9.   Sexton, L. T.; Horne, L. P.; Martin, C. R., Developing Synthetic Conical Nanopores for Biosensing Applications. *Molecular BioSystems* **2007,** *3*, 667-685.

10.   Bayley, H.; Martin, C. R., Resistive-Pulse Sensing-from Microbes to Molecules. *Chem. Rev.* **2000,** *100*, 2575-2594.

11.   Wanunu, M.; Sutin, J.; McNally, B.; Chow, A.; Meller, A., DNA Translocation Governed by Interactions with Solid-State Nanopores. *Biophys. J.* **2008,** *95*, 4716-4725.

12.   Aksimentiev, A., Deciphering Ionic Current Signatures of DNA Transport through a Nanopore. *Nanoscale* **2010,** *2*, 468-483.

13.   Smeets, R. M. M.; Keyser, U. F.; Krapf, D.; Wu, M.-Y.; Dekker, N. H.; Dekker, C., Salt Dependence of Ion Transport and DNA Translocation through Solid-State Nanopores. *Nano Lett.* **2006,** *6*, 89-95.

14.   Tabard-Cossa, V.; Trivedi, D.; Wiggin, M.; Jetha, N. N.; Marziali, A., Noise Analysis and Reduction in Solid-State Nanopores. *Nanotechnology* **2007,** *18*.

15.   Tabard-Cossa, V.; Wiggin, M.; Trivedi, D.; Jetha, N. N.; Dwyer, J. R.; Marziali, A., Single-Molecule Bonds Characterized by Solid-State Nanopore Force Spectroscopy. *ACS Nano* **2009,** *3*, 3009-3014.

16.   McNally, B.; Wanunu, M.; Meller, A., Electromechanical Unzipping of Individual DNA Molecules Using Synthetic Sub-2 Nm Pores. *Nano Lett.* **2008,** *8*, 3418-3422.

17.   Zhao, Q.; Sigalov, G.; Dimitrov, V.; Dorvel, B.; Mirsaidov, U.; Sligar, S.; Aksimentiev, A.; Timp, G., Detecting Snps Using a Synthetic Nanopore. *Nano Lett.* **2007,** *7*, 1680-1685.

18.   Liebes, Y.; Drozdov, M.; Avital, Y. Y.; Kauffmann, Y.; Rapaport, H.; Kaplan, W. D.; Ashkenasy, N., Reconstructing Solid State Nanopore Shape from Electrical Measurements. *Appl. Phys. Lett.* **2010,** *97*, 223105.

19.   Ayub, M.; Ivanov, A.; Instuli, E.; Cecchini, M.; Chansin, G.; McGilvery, C.; Hong, J.; Baldwin, G.; McComb, D.; Edel, J. B.; Albrecht, T., Nanopore/Electrode Structures for Single-Molecule Biosensing. *Electrochim. Acta* **2010,** *55*, 8237-8243.

20.   Stein, D.; Kruithof, M.; Dekker, C., Surface-Charge-Governed Ion Transport in Nanofluidic Channels. *Phys. Rev. Lett.* **2004,** *93*, 035901.

21.   Frament, C. M.; Dwyer, J. R., Conductance-Based Determination of Solid-State Nanopore Size and Shape: An Exploration of Performance Limits. *J. Phys. Chem. C* **2012,** *116*, 23315-23321.

22.   Kowalczyk, S. W.; Grosberg, A. Y.; Rabin, Y.; Dekker, C., Modeling the Conductance and DNA Blockade of Solid-State Nanopores. *Nanotechnology* **2011,** *22*, 315101.

23.   Frament, C. M.; Bandara, N.; Dwyer, J. R., Nanopore Surface Coating Delivers Nanopore Size and Shape through Conductance-Based Sizing. *ACS Appl. Mater. Interfaces* **2013,** *5*, 9330-9337.

24.   Makra, I.; Jágerszki, G.; Bitter, I.; Gyurcsányi, R. E., Nernst–Planck/Poisson Model for the Potential Response of Permselective Gold Nanopores. *Electrochim. Acta* **2012,** *73*, 70-77.

25.   Yang, J.; Ferranti, D. C.; Stern, L. A.; Sanford, C. A.; Huang, J.; Ren, Z.; Qin, L.-C.; Hall, A. R., Rapid and Precise Scanning Helium Ion Microscope Milling of Solid-State Nanopores for Biomolecule Detection. *Nanotechnology* **2011,** *22*, 285310.

26.   Li, J.; Stein, D.; McMullan, C.; Branton, D.; Aziz, M. J.; Golovchenko, J. A., Ion-Beam Sculpting at Nanometre Length Scales. *Nature* **2001,** *412*, 166-169.

27.   Storm, A. J.; Chen, J. H.; Ling, X. S.; Zandbergen, H. W.; Dekker, C., Fabrication of Solid-State Nanopores with Single-Nanometre Precision. *Nature Materials* **2003,** *2*, 537-540.

28.   Spinney, P. S.; Howitt, D. G.; Smith, R. L.; Collins, S. D., Nanopore Formation by Low-Energy Focused Electron Beam Machining. *Nanotechnology* **2010,** *21*, 375301.

29.   Kim, M. J.; McNally, B.; Murata, K.; Meller, A., Characteristics of Solid-State Nanometre Pores Fabricated Using a Transmission Electron Microscope. *Nanotechnology* **2007,** *18*.

30.   Kuan, A. T.; Golovchenko, J. A., Nanometer-Thin Solid-State Nanopores by Cold Ion Beam Sculpting. *Appl. Phys. Lett.* **2012,** *100*, 213104-213104.

31.   Wu, M.-Y.; Smeets, R. M. M.; Zandbergen, M.; Ziese, U.; Krapf, D.; Batson, P. E.; Dekker, N. H.; Dekker, C.; Zandbergen, H. W., Control of Shape and Material Composition of Solid-State Nanopores. *Nano Lett.* **2009,** *9*, 479-484.

32.   Vlassiouk, I.; Apel, P. Y.; Dmitriev, S. N.; Healy, K.; Siwy, Z. S., Versatile Ultrathin Nanoporous Silicon Nitride Membranes. *Proceedings of the National Academy of Sciences of the United States of America* **2009,** *106*, 21039-21044.

33.   Freedman, K. J.; Ahn, C. W.; Kim, M. J., Detection of Long and Short DNA Using Nanopores with Graphitic Polyhedral Edges. *ACS Nano* **2013,** *7*, 5008-5016.

34.   Wei, R.; Pedone, D.; Zürner, A.; Döblinger, M.; Rant, U., Fabrication of Metallized Nanopores in Silicon Nitride Membranes for Single-Molecule Sensing. *Small* **2010,** *6*, 1406-1414.

35.   Whelan, J. C.; Karawdeniya, B. I.; Bandara, Y. M. N. D. Y.; Velleco, B. D.; Masterson, C. M.; Dwyer, J. R., Electroless Plating of Thin Gold Films Directly onto Silicon Nitride Thin Films and into Micropores. *ACS Appl. Mater. Interfaces* **2014,** *6*, 10952-10957.

36.   Kwok, H.; Briggs, K.; Tabard-Cossa, V., Nanopore Fabrication by Controlled Dielectric Breakdown. *PLoS ONE* **2014,** *9*, e92880.

37.   Yusko, E. C.; Johnson, J. M.; Majd, S.; Prangkio, P.; Rollings, R. C.; Li, J.; Yang, J.; Mayer, M., Controlling Protein Translocation through Nanopores with Bio-Inspired Fluid Walls. *Nature Nanotechnology* **2011,** *6*, 253-260.

38.   Wanunu, M.; Meller, A., Chemically Modified Solid-State Nanopores. *Nano Lett.* **2007,** *7*, 1580-1585.

39.   Williams, K. R.; Muller, R. S., Etch Rates for Micromachining Processing. *J. Microelectromech. Syst.* **1996,** *5*, 256-269.

40.   Møller, P.; Nielsen, L. P., *Advanced Surface Technology*. Møller & Nielsen APS: Denmark, **2013**; Vol. 1, p 594.

41.   de Groot, G. W.; Santonicola, M. G.; Sugihara, K.; Zambelli, T.; Reimhult, E.; Vörös, J.; Vancso, G. J., Switching Transport through Nanopores with pH-Responsive Polymer Brushes for Controlled Ion Permeability. *ACS Appl. Mater. Interfaces* **2013,** *5*, 1400-1407.